Chapter 2

LOW COST SOLVOTHERMAL PROCESSED CTS QDs BASED BROADBAND (VISIBLE-NIR) PHOTOCONDUCTOR

This chapter include the low cost solvothermal synthesized Cu_2SnS_3 (CTS) QDs of average size ∼3.4 nm patterned over small spaced Ag contacts, thermally coated on glass substrate, to realize a Ag/CTS QDs/Ag based photoconductor structure. The optoelectronic characteristics of the fabricated photodetector is investigated under broad light (650-1100) illumination and the measurement of the device performance by calculating the optical parameters like Responsivity, Detectivity, Sensitivity, and Time response has been done *

*Parts of this chapter have been published in Sanjeev Mani Yadav, and Amritanshu Pandey. "Low Cost Solvothermal Processed CTS QDs (0D) Based Visible-NIR Photoconductor." *IEEE Sensors Journals* 21.18 (2021): 19978-19983

2.1 Introduction

Broadband visible-near infrared (Vis-NIR) photodetectors (PDs) with high sensitivity, responsivity and having low fabrication cost are indispensable these days due to their wide range of applications like imaging, chemical/biological sensing, environment sensing and in the field of optical fibre communication [194]. The broad range detection of light with good responsivity and sensitivity depends on the optical and electrical properties the active material used in the fabrication of the device. The traditional materials generally used for Vis-NIR detection are Si, SiGe, InGaAs etc. [28, 195] To realize high performance broadband photodetection from these materials the combination of multiple band photo sensitive materials is required [26]. The materials integration to realize large bandwidth photodetection not only increases the complexity and volume of photodetection system but also enhance the production cost [26]. The need for wide band detection have lead the researcher to explore some other class of materials and their nanostructures having higher absorption in broad range to facilitate broadband photodetection.

The emerging 2D materials such as MoS_2 and WS_2 have high absorption but only in narrow band [100]. The bandwidth enhancement has been achieved by combining 2D materials with low dimensional structure such as nanowires (1D) and quantum dots (0D). Due to quantum size effect [196, 197, 198], the optical and electrical property tunability based on its dimension is observed. The hybrid structure of these 2D/1D/0D nanostructures [199, 200, 201, 202, 203, 204] improve the optical performance of these detectors but introduce extra active material, structure complexity and enhance the overall fabrication cost. Now a days, 0D quantum dots nanostructure have been explored quite extensively due to its high absorption because of large surface to volume ratio.

The fabrication of broadband PDs based on quantum dots (QDs) are admired recently due to their size controlled detection capability, a wide and tunable absorption range and compatibility with various substrates [205]. The popular materials used for Vis-NIR broadband detection such as PbS, PbSe, CdTe, HgTe etc., [127, 128, 129] have

some limitations. PbS has inefficient carrier transfer due to long ligands decoration [133] whereas, HgTe and its QDs require large cooling system due to its poor stability in ambient condition [143]. Scarcity of Te is also an issue [151]. Further, QDs of PbS, Cd, Hg and Se are toxic in nature hence, find limited application in optoelectronic devices [206, 5, 207].

Recently, Cu_2SnS_3 (CTS) a highly stable, nontoxic, earth abundant [152, 153, 154] p-type semiconductor materials having high absorption coefficient 10^4 cm^{-1} is being investigated for PDs [5]. The CTS QDs have wide range of photodetection (Vis-NIR, 1.68–0.67 eV) [7] due to their large band gap tunability. The possibility of low cost synthesis method (solvothermal), non-hazardous and environment friendly nature of this material may result in a highly efficient broadband PD. The performance of photoconductor structures involving QDs film as a sole active material depends on many parameters including the quality (trap state density) and continuity of QDs film, mobility of majority carriers, channel spacing, and long insulating ligands used in the synthesis of QDs [208, 209, 210]. The small channel length between the electrodes is proposed to reduce these problems in our fabricated device.

Accordingly, a low cost CTS QDs based photoconductor fabricated over glass substrate is being reported. This small channel length ($\sim$63.3μm), compare to previous reports [105, 157], Ag/CTS QDs/Ag photoconductive type structure significantly improved the continuity of agglomerated QDs film and helped to transport the carriers effectively [211]. In results, the proposed structure shows huge improvement in the time responses in compare to previously reported CTS based detectors with good responsivity, detectivity and EQE. The further scaling down of the structure is possible by using some lithography techniques. We have fabricated our device using shadow mask technique of metal deposition at some tens of micrometer scale suitable for mass production of devices with low fabrication complexity.

2.2 Experimental Details

2.2.1 Synthesis of CTS QDs

CTS QDs used in this study has been synthesized by solvothermal technique as discussed in reports [5, 23]. In brief a solution of 0.3 mmol of $SnCl_2.2H_20$, 0.62 mmol of $CuCl_2.2H_20$ and 1.6 M PVP (as capping agent) was prepared in 20 ml of ethylene glycol. Another solution of 0.93 mmol of Na_2S was prepared in 20 ml of ethylene glycol. In next step the prepared Na_2S solution was added drop-wise in the first solution along with continuous magnetic stirring and results a brownish black solution. The resultant brownish black solution was transferred to a 50 ml autoclave and kept at 180^{o}C for 12h. The obtained product was then centrifuge and washed several times with ethanol and DI water and used for further characterizations after vacuum-dried. The schematic of solvothermal processed CTS QDs are shown in Fig.2.1.

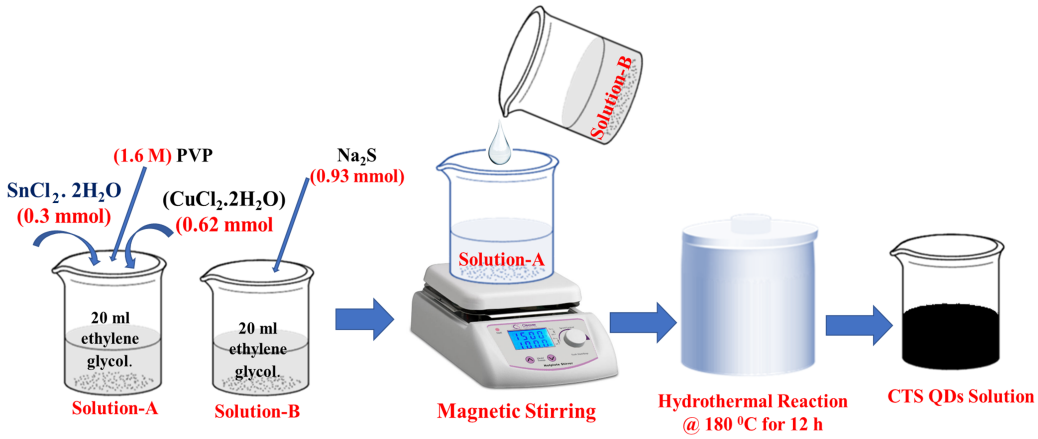

Figure 2.1: Solvothermal synthesis process to synthesize CTS QDs

2.2.2 Device Fabrication

CTS QDs have been synthesized by the solvothermal method as per the literature [5, 23]. The device fabrication includes mainly three steps. In first step, the cleaning of glass substrates (Area= 15×15 mm^2, thickness = 1 mm) has been performed by standard technique. In next step the Ag (99.99% pure) material was thermally evaporated in

vacuum coating unit and Ag contacts of thickness ∼90 nm with area (1×10 mm^2) was patterned on glass substrate by using masking as shown in device fabrication steps in Fig.2.2 (a). In final step, 40 mg of synthesized CTS QDs was dispersed in 1 ml of ethanol. The homogeneous dispersed solution (80μl) of CTS QDs was then drop casted over Ag patterned glass substrate having channel length 63.3μm. The resultant structure was then dried at 40^{o}C for 15 min. This drop cast and dry process were repeated one more time to ensure the film continuity over glass substrate. The resultant Ag/CTS QDs/Ag structure is shown in Fig.2.2 (b). The optical image (Fig. 2.2 (c)) of the device confirms the channel length of ∼63.3μm between two Ag contacts and results a photoconductive type structure.

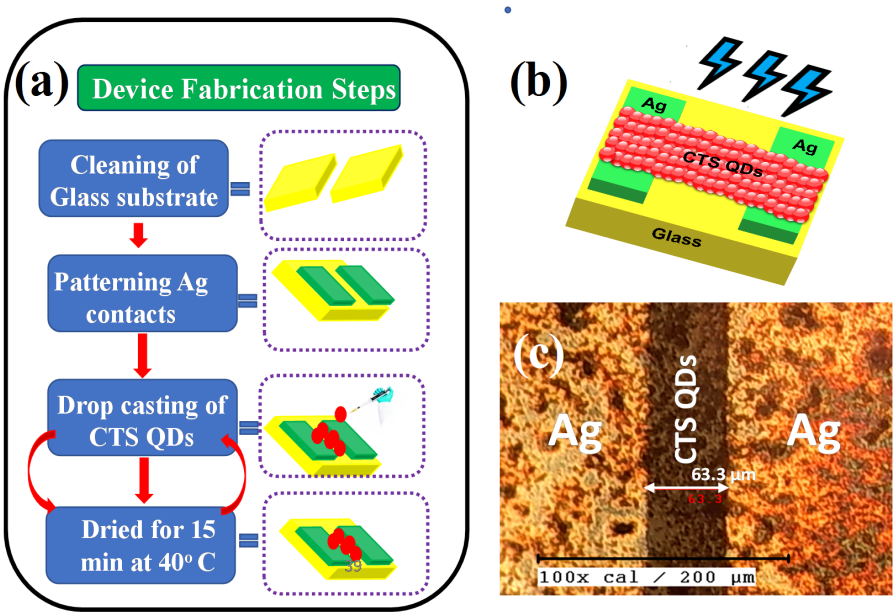

Figure 2.2: (a) Fabrication steps to realize a low cost Ag/CTS QDs/Ag photoconductor over glass substrate, (b) Fabricated device structure (c) Optical image of the fabricated device with marked channel dimension.

2.3 Results and Discussion

2.3.1 Structural Characterization of CTS QDs

The X-ray diffraction (X-RD) pattern (Fig.2.3 (a)) of solvothermal synthesized CTS QDs shows the multiple crystalline plane and confirms the tetragonal phase structure

[5, 23]. The transmission electron microscopy (TEM) image (Fig.2.3 (b)) of CTS QDs shows the agglomerated CTS QDs at larger scale along with Selected area electron diffraction (SAED) pattern with multiple rings. The obtained SAED pattern confirm the poly-crystalline nature of CTS and hold good agreement with its X-RD pattern. In addition to confirm the surface morphology, size of CTS QDs and the thickness of QDs film over glass substrate the structural characterizations have been performed. Fig.2.3 (c) shows the magnified TEM image of CTS QDs along with their size variation realized by its histogram (Inset). The diameter of CTS QDs was found to be ∼3.4 nm, less than the size of Bohr radius [68] and confirms the confinement phenomenon. The Field emission scanning electron microscopy (FE-SEM) image confirms the presence of CTS QDs and provide the surface morphology of CTS QDs as shown in Fig.2.3 (d). Further elemental mapping for FE-SEM image has been carried out by energy dispersive X-ray (EDX) analysis to confirm the presence of Cu, S, and Sn elements. Fig.2.3 (e) shows the atomic force microscopy (AFM) image of agglomerated CTS QDs distributed over glass substrate. The thickness of the CTS QDs film over glass substrate has been determined by the AFM image shown in Fig.2.3 (f) and was found to be ∼100 nm.

2.3.2 Optical and Electrical Characterizations of Device

The broadband (Vis-NIR) absorption of the synthesized CTS QDs has been observed using spectrometer (JAS.CO:V-730) and is given in Fig.2.4 (a). The cyclic voltammetry (C-V) measurement (Fig.2.4 (b)) of solvothermal synthesized CTS QDs has been also performed to estimate its bandgap as per the reports [5, 23]. In brief, the C-V scan has been performed with the help of three electrode methods. The three-electrode are Ag/AgCl (reference electrode), Pt (counter electrode) and glassy carbon (working electrode). For C-V scan all three electrodes were placed in KOH (0.1M) in the DI water electrolyte, and the QDs sample was drop casted on working electrode. A cyclic voltammetry scan is kept between -0.2 to 1.6 V with the scan rate of 0.1 V/s as shown in Fig.2.4 (b). The oxidation and reduction potential from the C-V plot were found to be 1.23 and 0.03 V, respectively. Finally, as per the equations reported in literature [5] relating the HOMO and LUMO levels with the oxidation and reduction potential has

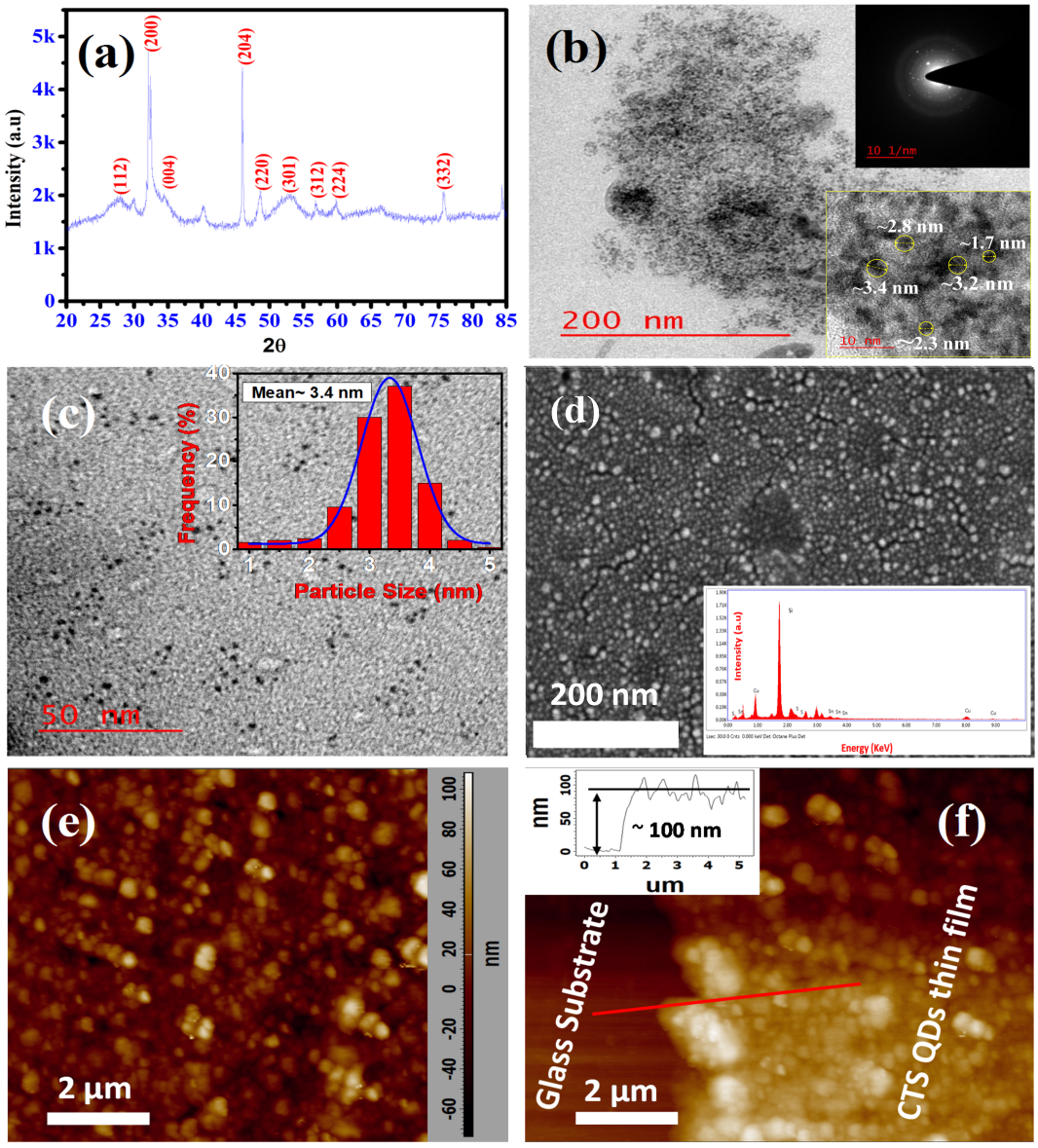

Figure 2.3: (a) XRD pattern of CTS QDs (b) TEM image along with SAED pattern (Inset) (c) Magnified TEM image of synthesized CTS QDs along with histogram plot relating size of QDs vs frequency(%) (Inset) with average size ∼3.4 nm, (d) FE-SEM image of CTS QDs and the corresponding Cu, Sn and S element mapping, (e) AFM image of agglomerated CTS QDs over glass substrate, (f) Height profile of CTS QDs film with estimated height ∼100 nm

been used to estimate the electrochemical band gap of CTS QDs. The electrochemical band gap of CTS QDs was found to be ∼ 1.2 eV which confirm the potentiality of CTS QDs as an active material for NIR regions. The I-V response (Fig.2.4 (c)) of the device

under dark and light illumination has been measured with the help of a parameter analyzer (Keysight: B1500A), a power meter (Thorlab: PM100D) and a light source along with monochromator (Princeton Instruments: SP2150i). The parameter analyzer in the above setup has been used to record the current for the variation of applied voltage under dark and illumination conditions. Power meter is used to measure the optical power density of the selected wavelength impinge on the device structure while monochromator is used to select the specific wavelength. The photo to dark current ratio (I_P/I_{dark}), named as sensitivity of the device, for visible (@730 nm ; @0.305 mW/cm^2) and NIR (@940 nm; 0.609 mW/cm^2) was found to be 2.28 and 8.2 respectively, at 5 V. The reported sensitivity of this device is found to be better than the previously reported CTS based nanostructure [63, 157] at low illumination power density.

The responsivity (R), external quantum efficiency EQE(%) and specific detectivity (D*) of the device for broad range illumination are shown in Fig.2.4 (d). The R of the device defined by (2.1) is found to be ∼67 and ∼37 mA/W for 940 and 730 nm illumination wavelengths respectively. The EQE of device related as (2.2) of the detector for visible range has been found to be more than ∼5% and reaches maximum ∼9% for NIR region. The (D*) of the detector if the short noise from dark current is the major contribution to the noise can be simplified as (2.3) and reported to be in the order of 10^{11} (Jones) for Vis-NIR illumination. In addition the maximum (D*) of the detector for Vis-NIR range is reported to be 1.69×10^{11} (Jones) and 3.047×10^{11} (Jones) for 730 and 940 nm illumination wavelengths respectively.

$$Responsivity(R) = \frac{I_p}{P_{opt}.S} \tag{2.1}$$

where I_P is photo current, P_{opt} is illuminated optical power density, S is effective illumination area (∼63.3×10^{-4} cm^2). The EQE of the detector is defined as

$$EQE = \frac{hc}{\lambda q}R =\sim \frac{1240}{\lambda(nm)}R \tag{2.2}$$

The specific detectivity of the device relates the responsivity (R) of the detector is

expressed as [212]

$$Detectivity(D^*) = \frac{R\sqrt{S}}{\sqrt{2qI_{dark}}} \tag{2.3}$$

where q is electronic charge and I_{dark} is dark current.

The reported R, EQE (%) and D^* of the device has been found much better than the CTS thin film-based detectors [63, 157], due to the higher absorption of CTS QDs which results from its higher surface-to-volume ratio in comparison to CTS nanosheets. In addition, the low channel length in the proposed structure also improves the current continuity and lead to the the efficient charge transportation. Furthermore, it is noted that the R, EQE (%) and D^* of this device with low optical power density has been found to be better than some other simple and hybrid Vis-NIR range detectors including PbS, HgTe and CdSeTe QDs nanostructures [213, 105, 214, 141, 215, 216, 217].

The time response of the device performed under Vis-NIR light source (Murphy Infrared, 150 W) with optical power density of $\sim$ 1 mW/cm^2 as shown in Fig.2.4 (e). Inset Fig.2.4 (e) shows the spectral response (Measured by spectrometer UCB 2000, Ocean Optics) of Vis-NIR light source with center wavelength @$\sim$710 nm. The ON and OFF time of the Vis-NIR light source is kept 10 and 10 s, respectively. For the illuminated power density (measured by Thorlabs PM100D power meter) the ON and OFF current in the device structure has been recorded with the help of a parameter analyzer (B1500A, Keysight). The rise and fall time from the observed current vs time characteristics has been measured by measuring the time taken by the current to reach 10%-90% (for rise time) and 90%-10% (for fall time) of its final value as shown in Fig.2.4 (f).

The rise time ($\sim$0.96 s) and fall time ($\sim$1.29 s) are comparatively the best reported speed parameters for CTS based broadband detectors [5, 23, 63, 157]. In addition, while comparing the time response parameters of our CTS QDs based device in compare to CTS based device [157] the improvement in the rise time is reported $\sim$91% while fall time improved by $\sim$67% by reducing the channel spacing from 80μm [157] to $\sim$63.3μm. The high improvement in these parameters are attributed to small electrodes (Ag) spacing i.e., 63.3μm. The small separation between the electrodes is responsible to reduce the time taken by the free charge carriers generated in CTS QDs to reach the

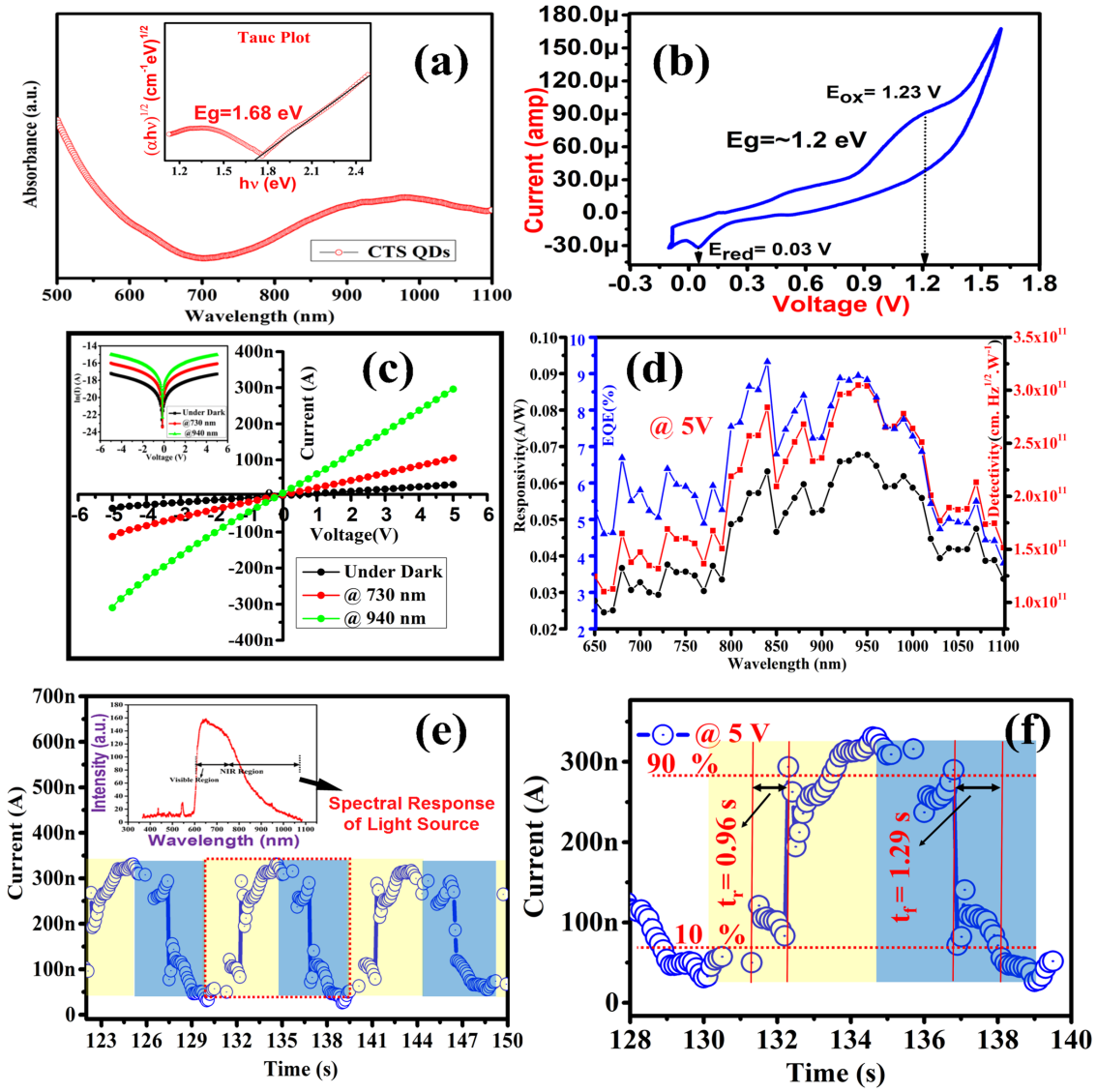

Figure 2.4: (a) Absorption spectra of solvothermal synthesized CTS QDs and Tauc plot (Inset) to estimate the optical band gap of CTS QDs (The optical band gap of CTS QDs is 1.68 eV), (b) Cyclic voltammetry (C-V) scan of the CTS QDs (The measured electrochemical bandgap of CTS QDs is ∼1.2 eV), (c) I-V characteristics of device under dark, 730 and 940 nm illumination wavelengths and ln(I)-V plot (Inset), (d) Responsivity (R), detectivity (D*) and EQE (%) of the device for broad spectral range illumination at 5 V, (e) Time response of the fabricated detector under Vis-NIR light source with spectral response (Inset), at 5V applied bias with ∼ 1 mW/cm^2 illuminated power density, (f) Rise (t_r) and fall (t_f) time calculation for the selected pulse as shown in Fig.2.4 (e)

electrodes under broad light illumination.

The time response of the device can be further improved by improving the quality

of QDs films which directly relate the trap state density and continuity of film in photoconductive type photodetection structure as discussed in recent reports [218, 219].

The superiority of the proposed photoconductor structure in compare to other broadband photodetectors has been summarized in Table-2.1 and 2.2.

Table 2.1: Comparison With Other Broadband Photodetectors

Device Structure	**Wavelength**	**Optical Power (mW/cm^2)**	**R (mA/W)**	**D (Jones)**	**EQE(%)**
This Paper	@730 nm	∼0.305	∼37	∼1.69×10^{11}	∼6.3
	@940 nm	∼0.609	∼67	∼3.047×10^{11}	∼8.9
Photoconductor [63]	750-1150 nm	∼286.6	10.17	3.2×10^{10}	2.29
	750-1150 nm	∼286.6	13.25	4.21×10^{10}	2.99
Photoconductor [157]	750-1100 nm	∼127.4/477.7	0.28	1.01×10^{9}	0.064
	750-1100 nm	∼127.4/477.7	0.49	1.72×10^{9}	0.109
Photoconductor[105]	@850 nm	@(0.068 mW)	1.22×10^{-5}	—-	—-
Photoconductor[141]	NIR	@(9W/mm^2)	∼3	—-	—-
Photoconductor[131]	800-1400 nm	0.43	$(1–7)\times10^{4}$	$(0.25–2)\times10^{11}$	—-
Hybrid [215]	@900 nm	2.55	∼11	4.2×10^{7}	∼1.51
Hybrid [216]	@1064 nm	—-	10	1.13×10^{10}	∼1.16
Hybrid [217]	@(300–800) nm	—-	∼ (1–15)	10^{10}–10^{11}	—-
Hybrid [220]	NIR	100	—-	$\sim10^{10}$	∼10
Photoconductor [221]	Vis-NIR	100	∼(10–33)	—-	∼ (2–10)
Photoconductor [132]	NIR	—-	$\leq3\times10^{4}$	$\leq2\times10^{10}$	—-
Hybrid [222]	300-1100	—-	0–730	$\leq2.2\times10^{12}$	∼(0-208)
Hybrid [120]	400-1100	@(53.75 nW/mm^2)	(1–3800)	$\leq2\times10^{14}$	—-
Hybrid [223]	400-700	—-	(0–15)	$\leq3\times10^{11}$	—-

Table 2.2: Time Response Comparison With CTS and Other Vis/NIR Photodetectors

Device Structure	**Channel Spacing (μm)**	**ON Time (s)**	**OFF Time (s)**
CTS QDs (This Paper)	63.3	0.96	1.29
CTS Nanostructures [157] (Photoconductor)	80	10.58	3.95
CTS Thin Films[63] (Photoconductor)	—-	5.99	13.58
CTS QDs/ITO-Glass[5] (Hybrid)	—-	8.6	1.9
CTS Nanostructures/PEDOT:PSS/ITO-PET[64] (Hybrid)	—-	4.9	4.6
CTS QDs/Graphene[23] (Hybrid)	—-	10.2	11.3
PbS QDs/Graphene[224] (Hybrid)	5–6	0.167	0.187
HgCdTe nanocrystals[221] (Photoconductor)	10	—-	0.337
Au/PbS QDs/Au[132] (Photoconductor)	5	0.16	3
MoS_2/UCNPs[225] (Hybrid)	<5	10–15	10–15
Chlorophyll-b/Si nanowire[222] (Hybrid)	—-	<1	<1
SnS_2/Si nanowire[120] (Hybrid)	—-	0.4	0.4

2.4 Principle of Operation

Under broad light illumination the CTS QDs of variable sizes absorb the light corresponding to their band gap (i.e., $E_g \sim 1/R^2$, here R is the dimension/size of QDs) and generate free charge carriers, as shown in energy band diagram of Fig.3.5 (a). In addition, Fig.3.5 (b) demonstrated the size dependent light absorption and generation of photocarriers of various size of CTS QDs over low cost glass substrate under vis-NIR illumination.

The linear I-V plot of the device (Fig.3.4 (c)) confirms the ohmic contact between Ag/CTS QDs as predicted theoretically [5].The photodetection mechanism of the device under illumination can be explained by in four sub-processes named as A, B, C and D in Fig.3.5 (c). When the photoconductor is illuminated with appropriate light energy, some photo-carriers are generated (sub-process A). Out of these photo charge carriers, the holes are transferred to the biased electrode and contribute to the photocurrent (sub-process B) while the electrons remain trapped in trap state as denoted by sub-process C [226, 227]. The trapped electrons in CTS QDs dis-balance the charge neutrality so holes from Ag contact must be injected into CTS QDs in equal amount as the trapped electron density (D_t) is noted as sub-process D. As a result, large current is obtained in Ag/CTS QDs/Ag photoconductor for Vis-NIR illumination. The photo current density (J_{ph}) in the photoconductor for an applied electric field E is given as $J_{ph} = e(\mu_n+\mu_p)\Delta pE + e\mu_p D_t E$ [9, 228, 226] where, first part represents the photocurrent due to generated photo carriers while the second term is due to the charge neutrality phenomenon. Further, the trapping of electrons will increase the recombination time of charge carriers hence, improves the optical characteristics of the device.

Therefore, large current due to high absorption of light by CTS QDs in Vis-NIR region and fast time response due to small channel length have been achieved in the fabricated device.

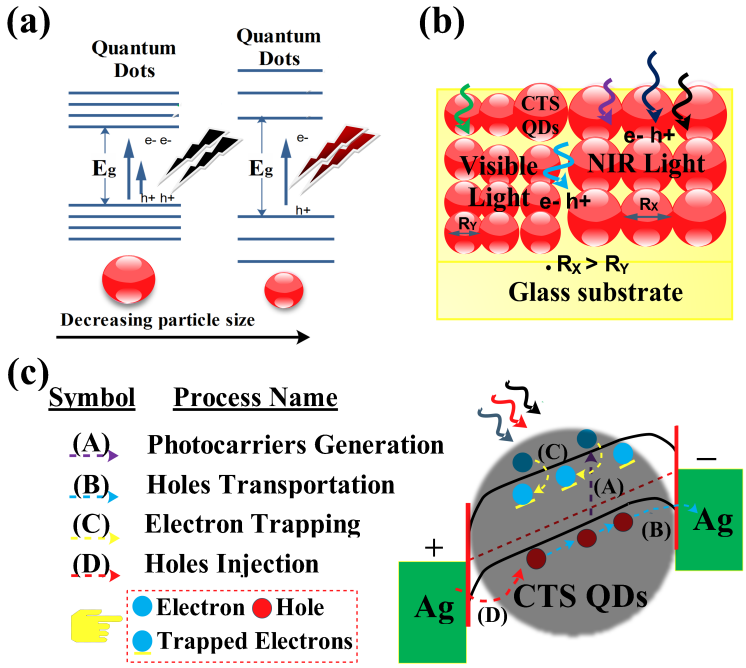

Figure 2.5: (a) Illustrations of QDs relating its energy band diagram with its size, (b) Size dependent light absorption by CTS QDs in visible and NIR spectrum, (c) Energy band diagram of Ag/p-CTS QDs/Ag under thermal equilibrium with applied bias along with illumination

2.5 Conclusion

This chapter reports probably first time the study of CTS QDs based photoconductive type photodetector. The optical characteristics of the device are measured for 650-1100 nm illumination wavelengths. The obtained R, D*, and EQE(%) of the device for 940 nm illumination wavelength are ~67 (mA/W), 3.047×10^{11} (Jones) and ~8.9% respectively. The time response (rise time ~0.96 s, fall time ~1.29 s) of the fabricated PD has been found to be better than the other CTS based PDs. The performance characteristics of the fabricated simple device structure are competitive with commercially available photodetectors based on Si, InGaAs, etc. In addition, the toxic free synthesis along with good thermal stability of CTS QDs gives a viable option of photodetection in this range.